Journal of Power Sources 180 (2008) 491–497

Contents lists available at ScienceDirect

Journal of Power Sources

journal homepage: www.elsevier.com/locate/jpowsour

Hydrogen storage properties of the Mg–Ti–H system prepared by high-energy–high-pressure reactive milling

Young Joon Choi, Jun Lu, Hong Yong Sohn*, Zhigang Zak Fang

Department of Metallurgical Engineering, University of Utah, 135 South 1460 East Room 412, Salt Lake City, UT 84112-0114, United States

ARTICLE INFO

Article history:
Received 12 January 2008
Received in revised form 5 February 2008
Accepted 6 February 2008
Available online 23 February 2008

Keywords:
Hydrogen storage
Magnesium hydride
Titanium hydride
Mechanical milling
Activation energy

ABSTRACT

Magnesium-based alloys are among the promising materials for hydrogen storage and fuel cell applications due to their high hydrogen content. In the present work, we investigated the hydrogen release/uptake properties of the Mg–Ti–H system. Samples were prepared from the mixtures of MgH_2 and TiH_2 in molar ratios of 7:1 and 4:1 using a high-energy-high-pressure (HEHP) mechanical ball-milling method under 13.8 MPa hydrogen pressure. Thermogravimetric analysis (TGA) showed that a relatively large amount of hydrogen (5.91 and 4.82 wt.%, respectively, for the above two samples) was released between 126 and 313 °C while temperature was increased at a heating rate of 5 °C min^{-1} under an argon flow. The onset dehydrogenation temperature of these mixtures, which is 126 °C, is much lower than that of MgH_2 alone, which is 381 °C. The activation energy of dehydrogenation was 71 kJ mol^{-1}, which is much smaller than that of as-received MgH_2 (153 kJ mol^{-1}) or as-milled MgH_2 (96 kJ mol^{-1}). Furthermore, the hydrogen capacity and the dehydrogenation temperature remained largely unchanged over five dehydrogenation and rehydrogenation cycles.

1. Introduction

Hydrogen is widely regarded as the most promising alternative energy source to replace fossil fuels as a clean energy carrier. It can be produced from a variety of renewable sources and yields a non-polluting waste, i.e. water. However, one of the key obstacles to the use of hydrogen as a fuel, especially for vehicles, is the lack of practical methods to store it on board. Because hydrogen is a gas under practical conditions, it is difficult to store it compactly and safely. Hydrogen storage systems developed so far are liquid hydrogen, compressed gas cylinders and solid-state storage materials. Compared to the physical approaches such as liquefaction and compression, hydrogen storage in the solid state has merits in terms of high volumetric and gravimetric hydrogen contents and, most importantly, safety [1]. Research in many laboratories around the world has focused on the solid-state hydrogen storage materials that are based on three primary approaches: (1) using inorganic solid hydride materials that have reversible dehydrogenation and rehydrogenation characteristics [2–9], (2) using the hydrolysis of alkali- and alkaline-earth metal hydrides and complex hydrides (such as MgH_2, LiH, $LiAlH_4$ and $LiBH_4$) [10,11] and (3) using carbon or other adsorbent materials to store hydrogen based on surface adsorption and desorption [12–14]. The critical characteristic properties of a solid hydrogen storage material include storage capacity, dehydrogenation temperature, plateau pressure and the reversibility of dehydrogenation and rehydrogenation. To meet the requirements of on-board storage for vehicles established by the U.S. Department of Energy, the storage capacity must be high, the kinetics of hydrogen release/uptake reactions must be satisfactory in an acceptable temperature range, and the reactions must be reversible under reasonable conditions [15].

Among the many different candidate materials based on metal hydrides, magnesium and magnesium-based alloys are considered very attractive candidates as rechargeable hydrogen storage materials because of their high hydrogen capacities (theoretically up to 7.6 wt.%), reversibility and low costs. However, the potential for practical use of MgH_2 is severely limited because of the poor rates of its hydrogen release/uptake reactions, especially at temperatures below 300 °C [16]. The poor kinetics is attributed to the fact that MgH_2 has strong ionically bound hydrogen, and thus is thermodynamically very stable within the temperature range that is practically useful. In another aspect, the equilibrium temperature T (1 bar) for MgH_2, defined as the minimum temperature required to reach 1 bar H_2 pressure during dehydrogenation, is 275 °C—too high for envisioned

* Corresponding author. Tel.: +1 801 581 5491; fax: +1 801 581 4937.
E-mail address: h.y.sohn@utah.edu (H.Y. Sohn).

0378-7753/$ – see front matter © 2008 Elsevier B.V. All rights reserved.
doi:10.1016/j.jpowsour.2008.02.038

practical vehicular applications [17]. Therefore, an important challenge for enabling MgH_2 for practical applications is to find a way to destabilize it to lower its dehydrogenation temperature.

In the past several decades, a great deal of research efforts has been reported in the literature to improve the hydrogen storage properties of MgH_2 [18–42]. There are several approaches for modifying MgH_2 such as reducing the particle size, doping it with catalytic materials, and more recently using thin film to synthesize binary or ternary magnesium-based metal hydrides. For instance, the hydrogen storage properties of Mg or MgH_2 doped with small amounts of transition metals (such as Ti, V, Mn, Fe, Co, Ni, Cu, and Pd) have been investigated to improve the hydrogenation/dehydrogenation kinetics without reducing its high hydrogen capacity [18,20–23,28,30,31,33,36,37]. Liang et al. reported that the hydrogen storage properties of MgH_2 can be improved with 5 mol.% of transition micro-particles of metals (Ti, V, Mn, Fe, and Ni). For example, a composite with V released ~5 wt.% hydrogen within 200 s at 300 °C under hydrogen pressure of 0.0015 MPa [20,21]. Zaluska et al. [18] have found that ~6 wt.% hydrogen was released at 330 °C within 30 min when MgH_2 was doped with 1 wt.% of transition metals Pd and Fe (corresponding to 0.3 mol.% of Pd and 0.5 mol.% of Fe).

One of the most notable results was reported by Hanada et al. [33]. They investigated the catalytic effect of nanoparticles of 3d-transition metals on the hydrogen storage properties of MgH_2. They found that the 2 mol.% Ni^{nano}-doped MgH_2 composite prepared by mechanical milling with short time and low rpm exhibited the most significant improvement of the kinetics of the dehydrogenation of MgH_2. It was shown that a large amount of hydrogen (6.5 wt.%) can be released in the temperature range from 150 to 250 °C at a heating rate of 5 °C min^{-1} under a He flow with a sufficiently low partial pressure of hydrogen [33]. Zaluska et al. [18] demonstrated that even a small amount of transition metal catalyst is sufficient for improving the reaction kinetics by the use of uniform mixture of metal nanoparticles and Mg/MgH_2 obtained by milling. Besides the transition metals, some transition metal oxides, fluorides and halides also showed positive catalytic effects on the dehydrogenation of MgH_2 [24,27,35,38,41].

Recently, it was reported that metastable alloys or ternary hydrides based on magnesium can be obtained using thin film deposition, which possesses unique hydrogen storage properties [29,39,40,42]. For example, Vermeulen et al. [39] reported that $Mg_yTi_{(1-y)}H$ thin film made by electron-beam deposition at room temperature, which has an fcc fluorite structure in contrast to the rutile structure of typical magnesium hydride, exhibited an enhanced electrochemical hydrogenation property superior to a Mg film. This is an encouraging result that has prompted many research groups to attempt to synthesize the same kinds of metastable phases in powder form, which were recently demonstrated by Kalisvaart et al. [43] and Rousselot et al. [44]. On the other hand, Kyoi et al. [29] have synthesized a new ternary magnesium-titanium hydride, Mg_7TiH_x, in a high-pressure anvil cell by reacting a mixture of MgH_2 and $TiH_{1.9}$ at 8 GPa and 873 K, which showed a better dehydrogenation property than binary magnesium or titanium hydrides.

Mechanical ball milling is well known to change various properties of materials, as a result of the formation of special microstructure, metastable phases, and modified surface. This technique has been found to be an effective way to improve the hydrogen release and uptake kinetics of metal hydrides. Hydrogenation properties are very sensitive to these modifications, and in some cases, substantial changes of the hydrogenation behavior can be obtained after milling. For example, the formation of nanocrystalline or amorphous structure produced by milling results in dramatic changes in hydrogenation properties, especially by eliminating the need for activation and improving hydrogenation/dehydrogenation kinetics [33,45,46].

In the present work, we investigated the feasibility of synthesizing Mg–Ti–H hydride systems using a high-energy-high-pressure (HEHP) mechanical milling method. The capability of HEHP milling for synthesizing hydride particles in a reactive atmosphere allows one to obtain nanoscaled materials without any formation of oxides. The synthesized Mg–Ti–H materials showed that the release and uptake of hydrogen are reversible with reasonable kinetics at a relatively low temperature.

2. Experimental apparatus and procedure

The initial materials, magnesium hydride (MgH_2, 98%) and titanium hydride (TiH_2, 99%), were purchased from Sigma–Aldrich (Milwaukee, WI) and Alfa-Aesar (Ward Hill, MA), respectively, and used as received without any further purification. All the material handling was carried out in a glove box filled with purified argon (99.999%) in the presence of an oxygen scavenger and a drying agent to prevent raw materials and samples from undergoing oxidation and/or hydroxide formation. Three grams of the mixtures of MgH_2 and TiH_2 in molar ratios of 7:1 and 4:1 were milled using an HEHP mill under 13.8 MPa hydrogen pressure. The weight ratio of balls to powder was 35:1 and the milling time was 12 h at room temperature.

The hydrogen release from the mixtures was examined by the use of a thermogravimetric analyzer (TGA, Shimadzu TGA50) in which 10 mg samples were heated under flowing argon up to 350 °C at a heating rate of 5 °C min^{-1} and then held at this temperature for a certain period of time. This equipment was placed inside the glovebox so that the TGA measurements could be achieved without exposing the samples to air. The hydrogenation properties of the mixtures $7MgH_2/TiH_2$ and $4MgH_2/TiH_2$ were evaluated by using a custom-made autoclave with a hydrogen pressure limit of 34.5 MPa at 500 °C. In the rehydrogenation process, 300 mg of the mixtures was held at 350 °C for 6 h under vacuum to ensure complete release of hydrogen, and then kept at 150 °C for 12 h under 10.3 MPa of hydrogen pressure for rehydrogenation.

The identification of phases in the reactants and products before and after the TGA was carried out using an X-ray diffractometer (XRD, Siemens D5000) with Ni-filtered Cu Kα radiation (λ = 1.5406 Å). Each sample for XRD analysis was mounted on a glass slide and covered with a Kapton® tape as a protective film in the glove box. The X-ray intensity was measured over diffraction angle 2θ from 10 to 100° with a scanning rate of 0.02° s^{-1}. Using the XRD peak broadening, the crystallite size and effective internal strain of sample were obtained by the Stokes and Wilson's formula [47].

A scanning electron microscope (SEM, TOPCON SM-300) equipped with energy dispersive X-ray spectrometry (EDS) was employed to observe the morphology of the samples before and after milling and determine the particle size. The samples were protected from exposure to air by a conductive tape in the glove box during the transfer to the SEM sample chamber.

For additional measurements of the particle size, a particle size analyzer (The Brookhaven Instruments ZetaPALS) which can detect the size range from 1 to 6000 nm was used. As the precision of the particle size analyzer is largely affected by the clarity of the carrier and dispersion of the particle in the liquid, the sample was suspended in heptane using an ultrasonic bath for several hours before the measurement.

A transmission electron microscope (TEM, FEI Tecnai 30) with an accelerating voltage of 120 kV was employed to further confirm the grain size of the sample. For the TEM observation, a dilute suspension was dropped onto a TEM grid, and dried.

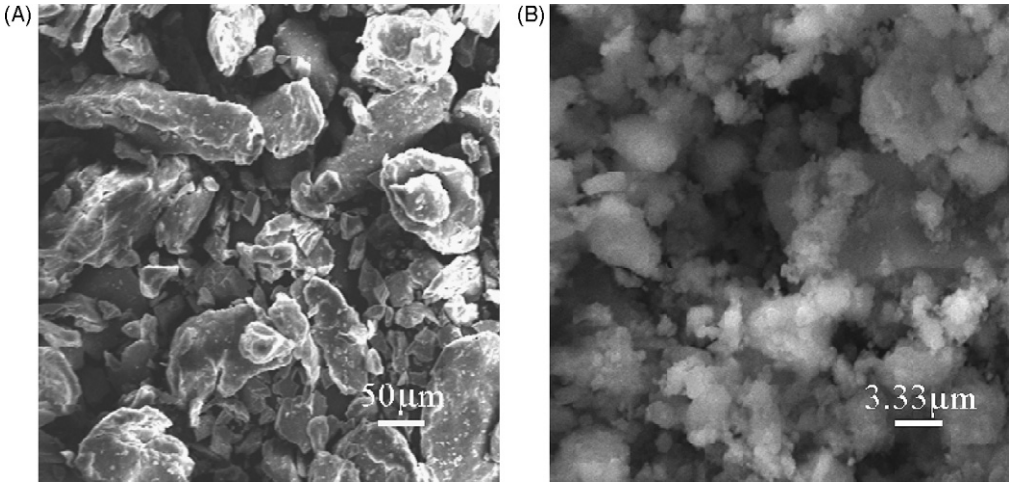

Fig. 1. SEM images of a mixture of (A) $7MgH_2/TiH_2$ before milling, and (B) $7MgH_2/TiH_2$ after 12 h milling under 13.8 MPa hydrogen pressure.

3. Results and discussion

3.1. Synthesis and characterization of the Mg–Ti–H system

In this work, the Mg–Ti–H system was first synthesized using an HEHP milling process under 13.8 MPa hydrogen pressure. The custom built planetary mill was applied not only for the preparation, doping or synthesis of powders by high-energy milling, but also to enhance the kinetics of dehydrogenation/rehydrogenation reactions. The high-energy planetary mill allowed the formation of highly defective and nanocrystalline storage materials as well as the synthesis of metastable phases of ternary metal hydrides such as the Na–Si–H system in our previous work. The results in that work showed that the most significant reduction in particle size occurred during the first 12 h of milling and this milling time induced sufficient contact between starting chemicals, i.e. further milling did not cause significant differences in the results. A hydrogen pressurized canister, which contains the Mg–Ti–H mixture or just MgH_2, was employed for the HEHP milling. Fig. 1 shows a typical SEM micrograph of the $7MgH_2/TiH_2$ mixed powder before and after milling. It shows that the particles before milling (Fig. 1(A)) have angular shapes and sizes in the range of 20–200 μm. Although the particles after milling (Fig. 1(B)) were aggregated, the sizes of the aggregated particles along with a small fraction of dispersed particles have been reduced to 0.3–6 μm. The atomic ratio of Mg and Ti in Fig. 1(B) is approximately 7:1 by EDS analysis using the Mg(K) and Ti(K) lines in the spectra, and no trace of Fe is detected. The image of EDS compositional mapping also shows a homogeneous distribution of TiH_2 among MgH_2 particles after milling.

A particle size analyzer, described earlier in Section 2, was used to measure the average particle size and the particle size distribution of the as-milled $7MgH_2/TiH_2$ mixed powder. Fig. 2 presents the particle size distribution as a lognormal function. It can be seen that the value of the average size is 390 nm and the minimum and maximum particle sizes are 168 and 902 nm, respectively.

Fig. 3 shows the XRD diffraction patterns of the $7MgH_2/TiH_2$ mixture. First of all, they indicate that the powder consisted of MgH_2 and TiH_2 as in the raw material. There is no indication of Fe which may come from the erosion of the milling tools and the formation of any new phases. More specifically, it can be concluded that under the experimental conditions of this study, there is no formation of the $Mg_7TiH_{\sim 16}$ phase. Secondly, XRD analyses in Fig. 3 show that after milling for 12 h, some of the peaks of MgH_2 and TiH_2 phases are absent, compared with that of MgH_2/TiH_2 before milling. This may be explained by the fact that the crystal structures of MgH_2 and TiH_2 phases were gradually weakened and deformed into amorphous structures upon milling. Finally, despite the presence of large particles, the as-milled $7MgH_2/TiH_2$ mixture presents broad diffraction peaks in the XRD pattern, as shown in Fig. 3(B), compared with that of $7MgH_2/TiH_2$ before milling, shown in Fig. 3(A). The broadening of diffraction peaks indicates the refinement of the crystallite size and the presence of the lattice micro strain in the as-

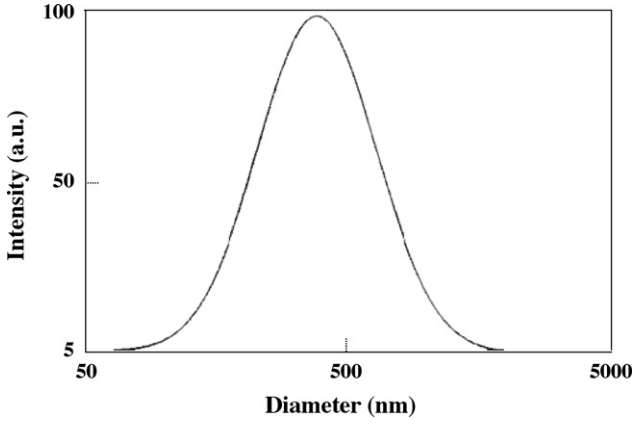

Fig. 2. Particle size distribution of the as-milled $7MgH_2/TiH_2$.

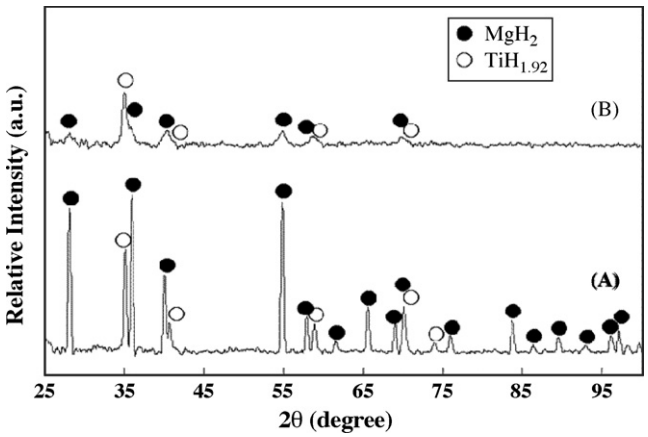

Fig. 3. XRD patterns of (A) $7MgH_2/TiH_2$ before milling, and (B) $7MgH_2/TiH_2$ after milling.

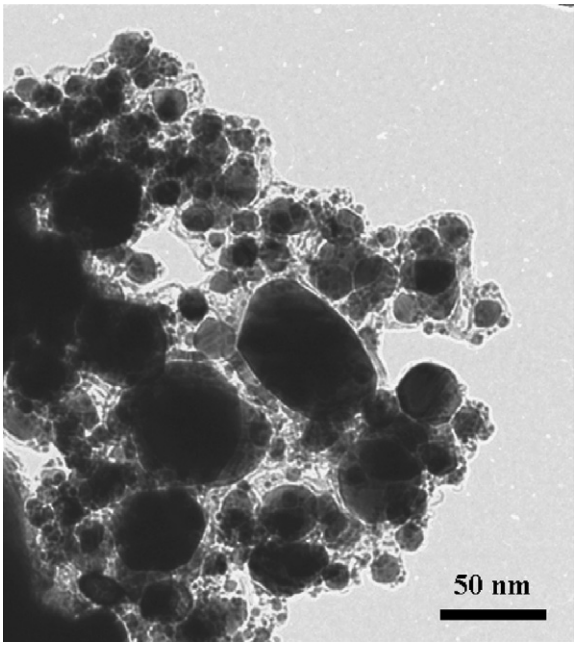

Fig. 4. TEM image of the as-milled $7MgH_2/TiH_2$.

milled $7MgH_2/TiH_2$ mixture. On the basis of the peak broadening, the grain size of $7MgH_2/TiH_2$ mixture after milling was estimated using the Stokes and Wilson's formula [47]. The average crystallite size of MgH_2 in the as-milled $7MgH_2/TiH_2$ mixture was 15 nm. This value was much smaller than that from SEM and particle size analyzer, mainly because the latter only measure the particle size rather than the crystallite size, and the particles after milling were aggregated. TEM is then used to further confirm the crystallite size obtained using the S–W formula. Fig. 4 shows a typical TEM image of the as-milled $7MgH_2/TiH_2$ mixture, in which an average crystallite size of about 23 nm was observed. This value is comparable to that calculated using the S–W formula.

It is also worthwhile to point out that no MgO peaks were detected in the mixture after HEHP milling. Magnesium oxide, which was reported to form during milling, causes the degradation of hydrogen capacity during the subsequent dehydrogenation and rehydrogenation cycles [21]. Thus, the milling method under pressurized reactive gas used in this study has the advantage of preventing reactants from oxidation during the process. The as-milled samples were then analyzed using TGA to study their dehydrogenation and rehydrogenation characteristics.

3.2. Hydrogen release/uptake behavior of the Mg–Ti–H system

It has been pointed out earlier that the rate of dehydrogenation of MgH_2 can be increased by using transition metals as catalysts in the form of metallic nanoparticles dispersed on MgH_2 particle surface [18,20–23,25,28,30,31,36,37]. To demonstrate the effects of additives and mechanical milling, Fig. 5 shows the TGA profiles for the as-milled $7MgH_2/TiH_2$ mixture, as-milled MgH_2, and as-received MgH_2. The TGA experiment was run under an argon atmosphere at a heating rate of 5 °C min^{-1} up to 350 °C, after which the temperature was held at this value for 1 h. It is seen that there are substantial differences in the onset temperature of dehydrogenation and time for complete hydrogen release for the two as-milled samples ($7MgH_2/TiH_2$ and MgH_2). The result shows that the hydrogen started to be released at about 126 °C and the weight loss accelerated at about 200 °C for the as-milled $7MgH_2/TiH_2$ sample. It shows that the temperature is considerably lower and the time is considerably shorter to complete hydrogen release from the

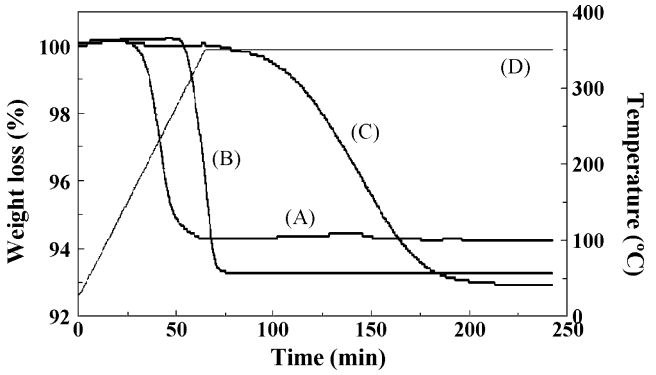

Fig. 5. TGA results for (A) as-milled $7MgH_2/TiH_2$, (B) as-milled MgH_2, and (C) as-received MgH_2 with a heating rate of 5°C min^{-1} up to 350 °C and holding for 1 h. Curve (D) shows the temperature profile corresponding to curves (A)–(C).

as-milled MgH_2 than from the un-milled, as-received MgH_2. More importantly, it is noted that the as-milled $7MgH_2/TiH_2$ releases nearly 100% of hydrogen within 60 min by the time the temperature reaches only 313 °C, indicating a significant improvement of the kinetics compared to either as-received or as-milled MgH_2.

The onset temperature is more easily shown in Fig. 6, which is a plot of weight loss vs. temperature. It is seen that the onset temperature in the TGA curve of the as-milled $7MgH_2/TiH_2$ (curve A) is approximately 255 and 144 °C lower than those of as-received MgH_2 (curve C) and as-milled MgH_2 (curve B), respectively.

The total weight loss amounted to 5.91 wt.% of the initial weight, which takes place within the temperature range from 126 to 313 °C. Assuming all the weight losses were due to the release of hydrogen, the dehydrogenation can be described as:

$$7MgH_2 + TiH_2 = 7Mg + TiH_2 + 7H_2 \quad (1)$$

The experimental weight loss is close to the theoretical hydrogen release of 5.98 wt.% from this reaction. In order to confirm if the dehydrogenation reaction indeed follows reaction (1), XRD analyses were conducted. Fig. 7 compares the XRD profiles of the $7MgH_2/TiH_2$ mixture before and after releasing hydrogen by heating to 350 °C and holding for 1 h. Crystalline phases were identified by comparing the experimental data with the JCPDS files from the International Center for Diffraction Data. Fig. 7(B) shows the XRD pattern of the sample after dehydrogenation. The peaks marked with (♦) represent the Mg phase and those marked with (○) are the TiH_2 phase. It is clearly seen that the products are a mixture of

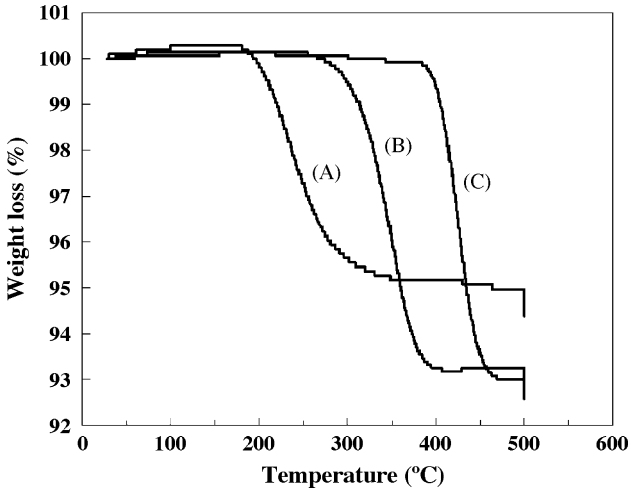

Fig. 6. Weight loss vs. temperature: (A) as-milled $7MgH_2/TiH_2$, (B) as-milled MgH_2, and (C) as-received MgH_2.

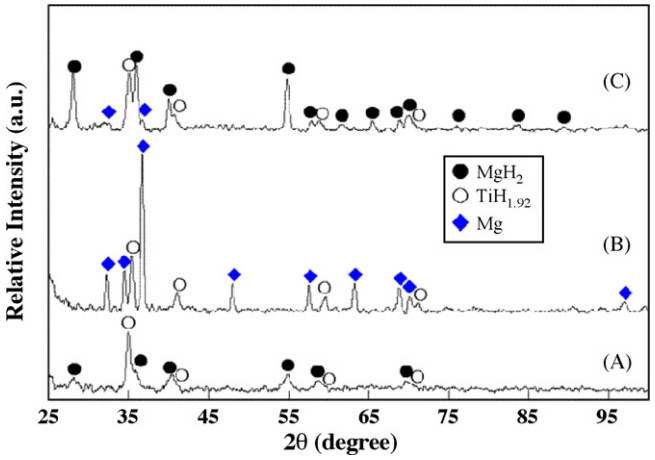

Fig. 7. XRD patterns of (A) as-milled $7MgH_2/TiH_2$, (B) dehydrogenated products of as-milled $7MgH_2/TiH_2$, and (C) hydrogenated products of dehydrogenated $7Mg/TiH_2$. [The amorphous-like broad peak is from a Kapton® tape used to cover the powders.]

Mg and TiH_2 and this suggests that the hydrogen release reaction under 350 °C from the as-milled $7MgH_2/TiH_2$ can be expressed by reaction (1).

A separate TGA result (not shown here) showed additional hydrogen release above 400 °C, according to:

$$TiH_2 = Ti + H_2 \quad (2)$$

This step, which is outside the temperature range considered in this study, contains another 0.86 wt.% of hydrogen making the overall theoretical capacity 6.84 wt.% for the $7MgH_2/TiH_2$ mixture, according to the following overall reaction:

$$7MgH_2 + TiH_2 = 7Mg + Ti + 8H_2 \quad (3)$$

In order to test the reversibility of the Mg–Ti–H system, the dehydrogenated products of reaction (1), was hydrogenated by using a custom-made autoclave under 10.3 MPa hydrogen pressure and 150 °C for 12 h. The hydrogenated product was analyzed using XRD and TGA. The XRD profile of hydrogenated products of dehydrogenated $7Mg/TiH_2$ is shown in Fig. 7(C), which suggests that the hydrogenation reaction was carried out successfully at the above experimental conditions. Fig. 8 shows the TGA profiles of the hydrogenated sample which indicates that the sample took up hydrogen amounting to about 5.61 wt.% of the hydrogenated products. It can be seen that the TGA profiles for the sample after the initial milling and after five cycles of dehydrogenation and rehydrogenation have almost the same shape and only a small amount of degradation amounting to a weight loss of 0.3 wt.% compared with the initially as-milled one was found. In other words, the hydrogen capacity and the starting hydrogen release temperature remained largely unchanged over five dehydrogenation and rehydrogenation cycles.

3.3. Kinetic analysis of the dehydrogenation reaction

Non-isothermal runs described above were performed to determine the activation energy for reaction (1) by using the Ozawa–Flynn–Wall method [48–50]. TGA profiles of the as-milled $7MgH_2/TiH_2$ mixture under various heating rates are shown in Fig. 9. The method is based on the following rate equation:

$$\frac{d\alpha}{dt} = Af(\alpha)\exp\left(\frac{-E_a}{RT}\right) \quad (4)$$

where α is the fractional conversion, t the reaction time, A the pre-exponential factor of the Arrhenius equation, $f(\alpha)$ a kinetic function that is related to the reaction mechanism and R the gas constant. Integration of Eq. (1) and the subsequent approximation under the condition with constant heating rate ($T = T_0 + \beta t$; β = the heating rate; T_0 = the starting temperature) result in the following equation:

$$\log\beta = -\frac{0.457E_a}{RT} - 2.315 - \log\left(\frac{R}{AE_a}\int_0^a \frac{d\alpha}{f(\alpha)}\right) \quad (5)$$

Based on Eq. (5), the activation energy, E_a, can be calculated from the slope of a plot of $\log\beta$ vs. $1/T$ at a given value of α.

According to the results in Fig. 9, the TGA profiles of the as-milled $7MgH_2/TiH_2$ move to a higher temperature with increasing heating rate from 1 to 20 °C min^{-1}, as expected. The activation energy is then evaluated using the heating rates (β = 1, 2, 5, 10 and 20 °C min^{-1}) and a fractional conversion (α = 0.4) from the TGA profiles by plotting $\log\beta$ vs. $1/T$. Fig. 10 presents the results for the dehydrogenation of (A) as-milled $7MgH_2/TiH_2$, (B) as-milled $4MgH_2/TiH_2$, (C) as-milled MgH_2, and (D) as-received MgH_2. The results show that the activation energy (E_a) for the dehydrogenation of the as-milled $7MgH_2/TiH_2$ is approximately 71 kJ mol^{-1}, which is much lower than the results determined for the as-received MgH_2 (153 kJ mol^{-1}) and as-milled MgH_2 (96 kJ mol^{-1}), respectively. The activation energy is further reduced to 68 kJ mol^{-1} when the molar ratio Mg:Ti was decreased from 7:1 to 4:1, which unfortunately causes the decline of hydrogen storage capacity from 5.91 to 4.82 wt.%.

The effect of TiH_2 may be due to its ability to destabilize MgH_2, similar to the observed effects of other elements. It has been

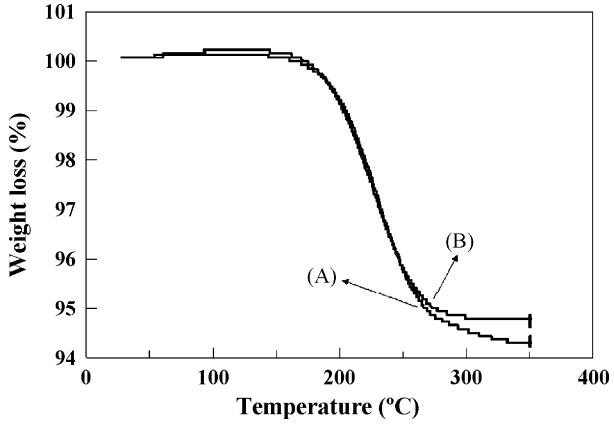

Fig. 8. TGA results for (A) $7MgH_2/TiH_2$ after the initial milling and (B) $7MgH_2/TiH_2$ after 5 cycles.

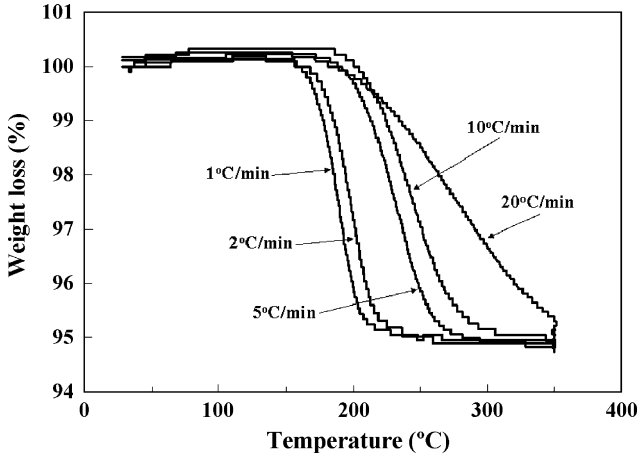

Fig. 9. TGA results for the as-milled $7MgH_2/TiH_2$ under various heating rates.

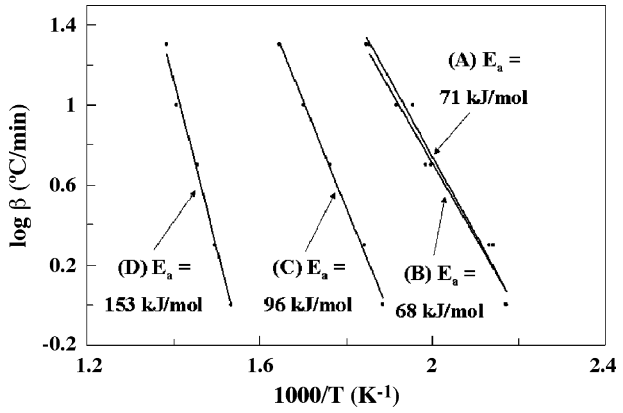

Fig. 10. Activation energy (E_a) for the dehydrogenation of (A) as-milled $7MgH_2/TiH_2$, (B) as-milled $4MgH_2/TiH_2$, (C) as-milled MgH_2, and (D) as-received MgH_2.

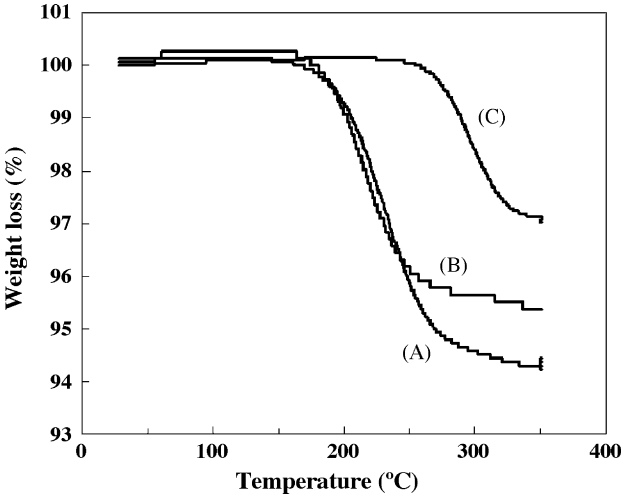

Fig. 11. Effect of different titanium compounds: (A) as-milled $7MgH_2/TiH_2$, (B) as-milled $7MgH_2/Ti$, and (C) as-milled $7MgH_2/TiCl_3$.

reported that MgH_2 can be destabilized by alloying with Si, which forms a more stable compound, Mg_2Si [32]. However, the MgH_2/Si system is kinetically limited in the rehydrogenation step. It has also been reported that with a small amount of doping with a 3d-transition metal, especially Ni nanoparticles, the dehydrogenation of MgH_2 took place at relatively lower temperatures [33]. The present work showed for the first time that the hydrogen release of MgH_2 can occur at a much lower temperature by the addition of TiH_2. In order to further understand the effect of TiH_2, different Ti species including Ti metal and $TiCl_3$ were used instead of TiH_2 in the same molar ratio to MgH_2. These mixtures were milled under the same condition as that of $7MgH_2/TiH_2$, and their dehydrogenation properties were then investigated by TGA. The results are shown in Fig. 11, which includes the TGA curve of as-milled $7MgH_2/TiH_2$ for comparison. It is clearly seen that the onset temperature of the dehydrogenation is increased when TiH_2 is replaced by Ti metal or $TiCl_3$.

4. Conclusions

In this work, the dehydrogenation of the Mg–Ti–H system prepared by a high-energy-high-pressure milling technique was investigated. The analyses of TGA and XRD data indicate that the $7MgH_2/TiH_2$ mixture decomposes into metallic Mg and TiH_2, releasing a large amount of hydrogen (5.91 wt.%) between 126 and 313 °C. This hydrogen release temperature is lower by about 255 °C than that of as-received MgH_2. The complete dehydrogenation of the $7MgH_2/TiH_2$ was achieved within 60 min at a heating rate of 5 °C min^{-1}, which is again much faster than that of MgH_2 under similar conditions. The hydrogenation experiment of the dehydrogenated sample proved that the properties of dehydrogenation reaction of the Mg–Ti–H system remained nearly unchanged after five cycles of dehydrogenation and rehydrogenation.

Acknowledgment

This research was supported by the financial support from the U.S. Department of Energy (DOE) under contract number DE-FC36-05GO15069.

References

[1] L. Schlapbach, A. Züttel, Nature 414 (2001) 353–358.
[2] B. Bogdanovic, M. Schwickardi, J. Alloys Compd. 253 (1997) 1–9.
[3] P. Chen, Z. Xiong, J. Luo, J. Lin, K.L. Tan, Nature 420 (2002) 302–304.
[4] J. Lu, Z.Z. Fang, J. Phys. Chem. B 109 (2005) 20830–20834.
[5] J. Lu, Z.Z. Fang, H.Y. Sohn, J. Phys. Chem. B 110 (2006) 14236–14239.
[6] J. Lu, Z.Z. Fang, H.Y. Sohn, Inorg. Chem. 45 (2006) 8749–8754.
[7] J. Lu, Z.Z. Fang, H.Y. Sohn, J. Power Sources 172 (2007) 853–858.
[8] J. Lu, Z.Z. Fang, Y.J. Choi, H.Y. Sohn, J. Phys. Chem. C 111 (2007) 12129–12134.
[9] J. Lu, Z.Z. Fang, H.Y. Sohn, R.C. Bowman Jr., S.-J. Hwang, J. Phys. Chem. C 111 (2007) 16686–16692.
[10] J.H. Leckey, L.E. Nulf, J.R. Kirkpatrick, Langmuir 12 (1996) 6361–6367.
[11] Y. Kojima, K.I. Suzuki, Y. Kawai, J. Mater. Sci. 39 (2004) 2227–2229.
[12] A.C. Dillon, K.M. Jones, T.A. Bekkedahl, C.H. Kiang, D.S. Bethune, M.J. Heben, Nature 386 (1997) 377–379.
[13] Y. Ye, C.C. Ahn, C. Witham, B. Fultz, J. Liu, A.G. Rinzler, D. Colbert, K.A. Smith, R.E. Smalley, Appl. Phys. Lett. 74 (1999) 2307–2309.
[14] P. Chen, X. Wu, J. Lin, K.L. Tan, Science 285 (1999) 91–93.
[15] U.S. Department of Energy, Multi-Year Research, Development and Demonstration Plan: Planned program activities for 2004–2015, http://www1.eere.energy.gov/hydrogenandfuelcells/mypp/.
[16] W. Grochala, P. Edwards, Chem. Rev. 104 (2004) 1283–1316.
[17] IEA/DOE/SNL Hydride Database available at the Hydride Information Center, Sandia National Laboratories Home Page, http://hydpark.ca.sandia.gov/.
[18] A. Zaluska, L. Zaluski, J.O. Ström-Olsen, J. Alloys Compd. 288 (1999) 217–225.
[19] A. Zaluska, L. Zaluski, J.O. Ström-Olsen, J. Alloys Compd. 289 (1999) 197–206.
[20] G. Liang, J. Huot, S. Boily, A.V. Neste, R. Schulz, J. Alloys Compd. 291 (1999) 295–299.
[21] G. Liang, J. Huot, S. Boily, A.V. Neste, R. Schulz, J. Alloys Compd. 292 (1999) 247–252.
[22] H. Reule, M. Hirscher, A. Weißhardt, H. Kronmuller, J. Alloys Compd. 305 (2000) 246–252.
[23] Z. Dehouche, J. Goyette, T.K. Bose, J. Huot, R. Schulz, Nano Lett. 1 (2001) 175–178.
[24] W. Oelerich, T. Klassen, R. Bormann, J. Alloys Compd. 315 (2001) 237–242.
[25] A. Zaluska, L. Zaluski, J.O. Ström-Olsen, Appl. Phys. A Mater. Sci. Process. 72 (2001) 157–165.
[26] P. Wang, H.F. Zhang, B.Z. Ding, Z.Q. Hu, Acta Mater. 49 (2001) 921–926.
[27] G. Barkhordarian, T. Klassen, R. Bormann, Scr. Mater. 49 (2003) 213–217.
[28] G. Liang, J. Alloys Compd. 370 (2004) 123–128.
[29] D. Kyoi, T. Sato, E. Rönnebro, N. Kitamura, A. Ueda, M. Ito, S. Katsuyama, S. Hara, D. Noréus, T. Sakai, J. Alloys Compd. 372 (2004) 213–217.
[30] J.F.R. De Castro, S.F. Santos, A.L.M. Costa, A.R. Yavari, W.J. Botta, T.T. Ishikawa, J. Alloys Compd. 376 (2004) 251–256.
[31] J. Charbonnier, P. de Rango, D. Fruchart, S. Miraglia, L. Pontonnier, S. Rivoirard, N. Skryabina, P. Vulliet, J. Alloys Compd. 383 (2004) 205–208.
[32] J.J. Vajo, F. Mertens, C.C. Ahn, R.C. Bowman Jr., B. Fultz, J. Phys. Chem. B 108 (2004) 13977–13983.
[33] N. Hanada, T. Ichikawa, H. Fujii, J. Phys. Chem. B 109 (2005) 7188–7194.
[34] S.R. Johnson, P.A. Anderson, P.P. Edwards, I. Gameson, J.W. Prendergast, M. Al-Mamouri, D. Book, I.R. Harris, J.D. Speight, A. Walton, Chem. Commun. (2005) 2823–2825.
[35] M.-Y. Song, D.R. Mumm, S.-N. Kwon, S.-H. Hong, J.-S. Bae, J. Alloys Compd. 416 (2006) 239–244.
[36] G. Barkhordarian, T. Klassen, R. Bormann, J. Phys. Chem. B 110 (2006) 11020–11024.
[37] X. Yao, C. Wu, A. Du, G.Q. Lu, H. Cheng, S.C. Smith, J. Zou, Y. He, J. Phys. Chem. B 110 (2006) 11697–11703.
[38] V.V. Bhat, A. Rougier, L. Aymard, X. Darok, G. Nazri, J.M. Tarascon, J. Power Sources 159 (2006) 107–110.
[39] P. Vermeulen, R.A.H. Niessen, P.H.L. Notten, Electrochem. Commun. 8 (2006) 27–32.
[40] W.P. Kalisvaart, R.A.H. Niessen, P.H.L. Notten, J. Alloys Compd. 417 (2006) 280–291.
[41] S.-A. Jin, J.-H. Shim, Y.W. Cho, K.-W. Yi, J. Power Sources 172 (2007) 859–862.

[42] D. Kyoi, N. Kitamura, H. Tanaka, A. Ueda, S. Tanase, T. Sakai, J. Alloys Compd. 428 (2007) 268–273.
[43] W.P. Kalisvaart, H.J. Wondergem, F. Bakker, P.H.L. Notten, J. Mater. Res. 22 (2007) 1640–1649.
[44] S. Rousselot, M.-P. Bichat, D. Guay, L. Roué, J. Power Sources 175 (2008) 621–624.
[45] J. Huot, G. Liang, S. Boily, A. Van Neste, R. Schulz, J. Alloys Compd. 293–297 (1999) 495–500.
[46] G. Mulas, L. Schiffini, G. Tanda, G. Cocco, J. Alloys Compd. 404–406 (2005) 343–346.
[47] G.K. Williamson, W.H. Hall, Acta Metall. 1 (1953) 22–31.
[48] J.H. Flynn, L.A. Wall, J. Polym. Sci. Pt. B-Polym. Lett. 4 (1966) 323–328.
[49] T. Ozawa, J. Therm. Anal. 2 (1970) 301–324.
[50] C.R. Li, T.B. Tang, J. Mater. Sci. 34 (1999) 3467–3470.